Journal of Materials Chemistry A

ARTICLE

Rapid, Efficient Phase Pure Synthesis of CaAl-NO_3 Layered Double Hydroxide

Received 00th January 20xx,
Accepted 00th January 20xx

DOI: 10.1039/x0xx00000x

www.rsc.org/

Miaosen Yang, Emma Tuckley, Jean-Charles Buffet and Dermot O'Hare*

Phase pure Ca_2Al-NO_3-LDH nanoplatelets have been successfully synthesised by rapid mixing and precipitation from water in air using a coloidal mill. The as synthesised nanoplatelets have an average particle size of 250 nm (by TEM) compared to 2.4 μm via conventional coprecipitation. The Ca_2AlNO_3-LDH nanoplatelet suspensions are not stable, and age post synthesis. TEM data showed that the particles increase in size from 250 to 705 nm after 4 weeks at 8°C. TEM data also revealed that storage at lower temperatures (–20°C) significantly slows platelet growth. Aqueous suspensions of Ca_2AlNO_3-LDH nanoplates slowly decompose at room temperature.

Introduction

Layered Double Hydroxides (LDHs) are a family of compounds which commonly adopt the general formula $M^{2+}_{1-x}M^{3+}_x(OH)_2(A^{n-})_{x/n}.mH_2O$ (where M^{2+} and M^{3+} are metal cations, and A^{n-} is an interlayer anion).[1] The parent of this family of compounds is a naturally occurring mineral called hydrotalcite.[2] LDHs are a class of anionic clays with a structure based on brucite ($Mg(OH)_2$),[3] which is made up of edge sharing $Mg(OH)_6$ octahedral units.[4] In the LDHs some of the divalent M^{2+} cations are substituted for trivalent M^{3+} cations affording positively charged sheets. This charge is balanced by the intercalation of anions into the interlayer space. LDHs can be found with two different polymorphic structures.[5] The identities of the divalent (e.g. Ca^{2+}, Mg^{2+}, Fe^{2+}, Co^{2+}, Cu^{2+}, Ni^{2+}, or Zn^{2+}) and trivalent cations (e.g. Al^{3+}, Cr^{3+}, Ga^{3+}, In^{3+}, Mn^{3+} or Fe^{3+}) can be changed, as can the interlayer anion (A^{n-}).[6]

This flexibility in composition leads to a large range of LDHs with a variety of properties and applications include catalysis or catalyst precursors,[7,8,9] anion exchangers,[10] electro- and photo-active materials,[11-13] flame retardants,[14] absorbents,[15] and pharmaceuticals.[16,17] Specifically, hydrocalumite-like materials (CaAl-LDHs) have been used in catalysis,[18-23] and they also play several significant roles in cements (*e.g.* to accelerate or retard the hydration reaction).[24-25]

However, the synthesis of pure $[Ca_2Al(OH)_6](A^{n-})_{1/n}$ (CaAl-A LDHs) is still very challenging, as $CaCO_3$ precipitation under the basic pH conditions during LDH synthesis is so favourable. Vieille *et al*. have previously reported a method involving the use of a mixed water/ethanol solution to synthesize CaAl-LDHs at 65 °C under N_2 with decarbonated water.[26] Xu *et al.* improved on this approach by employing the separate nucleation and aging steps (SNAS) method.[25] Although it is possible to use Xu's method to synthesise CaAl-LDHs, the use of an organic solvent, the high temperature and long aging times make the process prohibitively expensive for large scale production. Very recently, Sánchez-Cantú and co-workers reported a new preparation method for hydrocalumite-like compounds with high phase purity under a helium flow.[27] Such synthesis complexities have severely limited the industrial use of CaAl-LDHs.

Here, we described a facile, cost effective and efficient route to synthesise Ca_2Al-NO_3 LDH via a rapid mixing method without using organic solvents, an N_2 atmosphere or a significant ageing time. We have also investigated long term ageing behaviour of Ca_2Al-LDH nanoparticle suspensions.

Results and Discussion

Phase pure synthesis of Ca_2Al-NO_3 LDH nanoplates

We have discovered that very rapid mixing followed by rapid precipitation is the key to an efficient and cost effective synthesis of $[Ca_2Al(OH)_6](NO_3)$ (Ca_2AlNO_3-LDH).[28] Very rapid addition of a 2:1 molar ratio of $Ca(NO_3)_2{\cdot}4H_2O$ and $Al(NO_3)_3{\cdot}9H_2O$ in deionised, degassed water to a 2.2 M NaOH solution using a colloid mail with a rotor speed of 2000 rpm for 90 s gives after water washing phase pure Ca_2AlNO_3-LDH. The powder X-ray (XRD) pattern of the LDH is shown in Fig. S1 exhibits the characteristic (*002*), (*004*), (*006*) Bragg reflections corresponding to the unit cell parameters of a reference Ca_2AlNO_3-LDH sample. Although the reaction was performed in air we see no evidence of any Bragg reflections due to $CaCO_3$. The FTIR, Fig S2, shows absorptions at ~3600 cm^{-1} (-OH and intercalated water), 1630 cm^{-1} (bending mode of water), 1400 and 1350 cm^{-1} (N-O stretching mode of the intercalated NO_3^-). The transmission electronic microscopy (TEM) and scanning electronic microscopy (SEM) images show that the

[a] *Chemistry Research Laboratory, Department of Chemistry, 12 Mansfield Road, OX1 3TA Oxford, UK. E-mail: dermot.ohare@chem.ox.ac.uk*

Electronic Supplementary Information (ESI) available: [X-ray powder, infra-red spectroscopy and particle sizes determination]. See DOI: 10.1039/x0xx00000x

Ca_2AlNO_3-LDH particles synthesised using this very rapid mixing method adopt a hexagonal plate like morphology (Fig. S3 and S4). The darker areas on the TEM image indicate stacking of the LDH sheets, or a thicker sheet. The average particle size was found to be 250 nm, with a large standard deviation of 106 nm. Thermogravimetric analysis (TGA) was used to analyse the thermal decomposition of the Ca_2AlNO_3-LDH (Fig. S5). The first weight loss between room temperature and 200 °C (T1) is due the loss of the physisorbed water either on the surface or in the interlayer galleries. The second weight loss which occurs between 200 and 450 °C (T2) is due to the loss of water from dehydroxylation of the inorganic layers. The third beyond 450 °C (T3) is due to the decomposition of the intercalated nitrate group (or other guest anions). The N_2 Brunauer–Emmett–Teller (BET) adsorption isotherm has a shape indicative of a microporous structure (Fig. S6). The as prepared Ca_2AlNO_3-LDH sample using 2000 rpm rotor speed has a surface area of 17.95 $m^2.g^{-1}$. The ^{27}Al solid state NMR spectrum shows one resonance peak at 10.05 ppm, consistent with a single aluminium environment in the sample (Fig. S7).[29]

Effects of rotor speed

We find that Ca_2AlNO_3-LDH samples prepared using different rotor speeds in the colloid mill have a different average platelet size (Fig. 1). Using a rotor speed of 2000 rpm the Ca_2AlNO_3-LDH platelets initially have an average diameter of 430 nm. However, when Ca_2AlNO_3-LDH is prepared using a colloidal mill rotor speed of 8000 rpm the initial LDH platelet diameter is 285 nm.

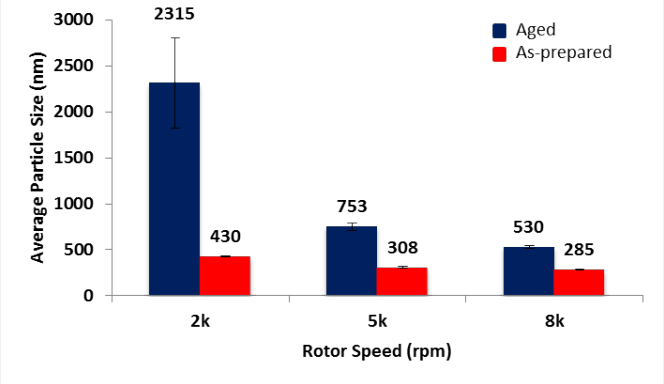

Fig. 1 Average particle size obtained from DLS for Ca_2AlNO_3-LDH samples stored at 8 °C for different times.

Storage studies of Ca_2AlNO_3-LDH nanoplatelet suspensions

Thick aqueous suspensions of the Ca_2AlNO_3-LDH nanoplatelets were stored at 8 °C and studies at different time periods to observe ageing effects on the nanoparticles. Fig S8 shows the average particle size over 4 weeks. Fig. 2 shows the evolution of the XRD of Ca_2AlNO_3-LDH nanoplatelets after 4 weeks. No new Bragg reflections are observed but it is clear that the crystallinity of the sample is increasing. The average crystallite size (or the mean crystallite domain length (CDL) along the *a*-, *b*- and *c*-axes) can be calculated from the full width at half maximum (FWHM) of the Bragg reflections using the Scherrer equation.[30] We find that the CDL along the *c*-axis increases from 143 to 717 Å after 4 weeks (Table S1). This is an important discovery since particle size is an important aspect for the function of Ca_2AlNO_3-LDHs in cement technology. Thus the temporal evolution of Ca_2AlNO_3-LDH pastes was studies in detail.[24]

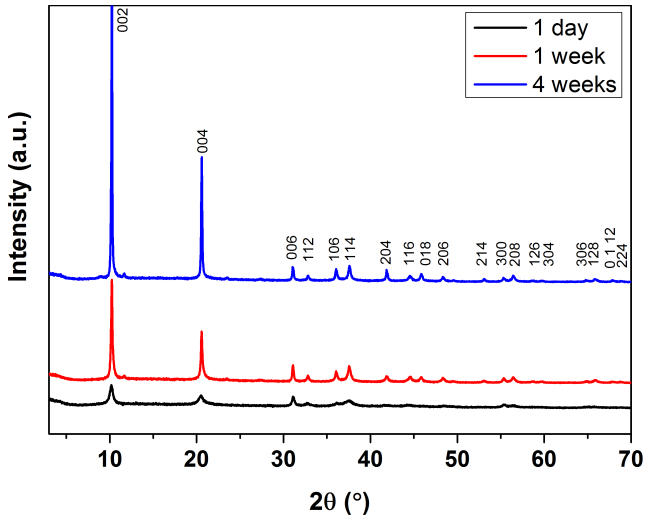

Fig. 2 XRD data for Ca_2AlNO_3 nanoplatelet suspensions after different storage times at 8 °C.

The average particle sizes calculated from the TEM images confirms an increase in the average particle size when this LDH is aged at 8 °C. The average platelet size increases from 250 to 705 nm after 4 weeks. In addition, the morphology of the platelets begins to change (Fig. 3). Immediately after synthesis most of the Ca_2AlNO_3-LDH particles adopt a hexagonal plate-like morphology (circled in blue). Upon storage, the particles begin to grow in the *ab*-plane forming parallelogram shaped platelets (circled in magenta). This may be because the surface energy of one face is lower than another under these conditions, so the particles grow preferentially in this plane. The TEM images of the LDHs that have been stored for 4 weeks show a 3D diamond-like morphology (circled in red).

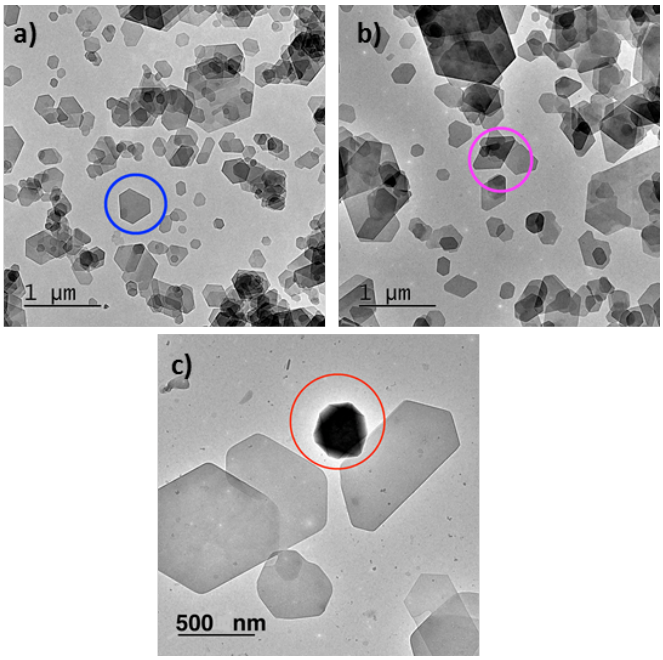

Fig. 3 TEM images for Ca_2AlNO_3-LDH nanoplatelets (a) immediately after synthesis, (b) after storage for 1 week at 8 °C and (c) after storage for 4 weeks at 8 °C.

Scanning electron microscopy (SEM) was also be used to study the particle morphology. The morphology of the sample immediately post synthesis had well defined hexagonal plate-like structure, (Fig. S4). The morphology of the sample after storage appears significantly less defined, Fig. 4.

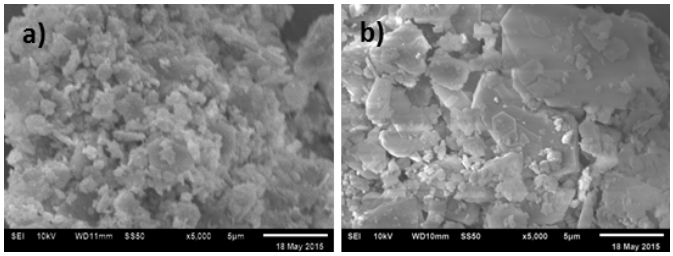

Fig. 4 SEM images of Ca_2AlNO_3-LDH after storage (a) 1 week at 8 °C and (b) 4 weeks at 8 °C.

Fig. 5 shows a very significant increase in particle size on storage with an increase from an initial value of 430 to 1865 nm after storage for 1 week at 8 °C to 2461 nm after 4 weeks, the standard deviation of the average particle size also increases from 8 to 188 nm in this time.

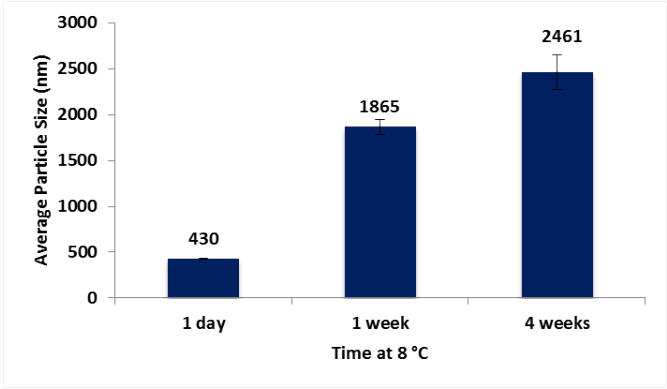

Fig. 5 Average particle size for Ca_2AlNO_3-LDH nanoplatelets after storage at 8 °C for 1 day, 1 week and 4 weeks.

Remarkably, we also find that Ca_2AlNO_3-LDH samples prepared using different mixing speeds in the colloid mill age at different rates (Fig. 1). Using a rotor speed of 2000 rpm the Ca_2AlNO_3-LDH platelets initially have an average diameter of 430 nm but these increase to 2315 nm upon aging at 8 °C for 4 weeks. While Ca_2AlNO_3-LDH prepared using a colloidal mill rotor speed of 8000 rpm initially produces 285 nm platelets grow to 530 nm after 4 weeks.

Variation in storage temperature

To investigate how temperature affects the rate of growth and change in morphology of these LDH suspensions Ca_2AlNO_3-LDH nanoplatelets synthesised by rapid mixing were stored for 1 week at different temperatures. The XRD patterns show a broadening of the Bragg reflections upon aging at 23 °C compared to 8 °C, consistent with an decrease in crystallinity (Fig. S9). The CDL along the *c*-axis are 143, 483 and 303 Å for the samples aged at –20, 8 and 23 °C respectively.

The Ca_2AlNO_3-LDH platelets appear to grow less rapidly at room temperature (23 °C) than at 8 °C, which is surprising. We attribute this to a decrease in the overall average due to increasing presence of impurities. The XRD pattern for Ca_2AlNO_3-LDH after storage for 1 week at 23 °C appears to become impure as extra Bragg reflections are observed. This indicates that the Ca_2AlNO_3-LDHs nanoplatelet suspensions in water are not stable at room temperature and begin to decompose which has a negative effect on particle growth. This may explain why Ca_2AlNO_3-LDH stored at 8 °C is more crystalline than a sample stored at 23 °C.

Changes in the particle size were also studied using TEM. These data suggest an increase in particle size with increased storage temperature (Fig. S10). Platelets stored at –20 °C for 1 week had an average particle size of 199 nm, while another batch of platelets stored at 23 °C had an average size of 415 nm. The standard deviation in the platelets size increased as storage temperature increased demonstrating a loss of control on the average particle size. The TEM images also revealed changes in the particle morphology. The platelets stored at –20 °C were uniform in shape (Fig. 6), while the particles stored at 8 °C although are well defined have a larger variation in sizes (Fig. 3). The particles stored at 23 °C appear

much less well defined and exhibit impurities (Fig. 6), as indicated by the XRD data.

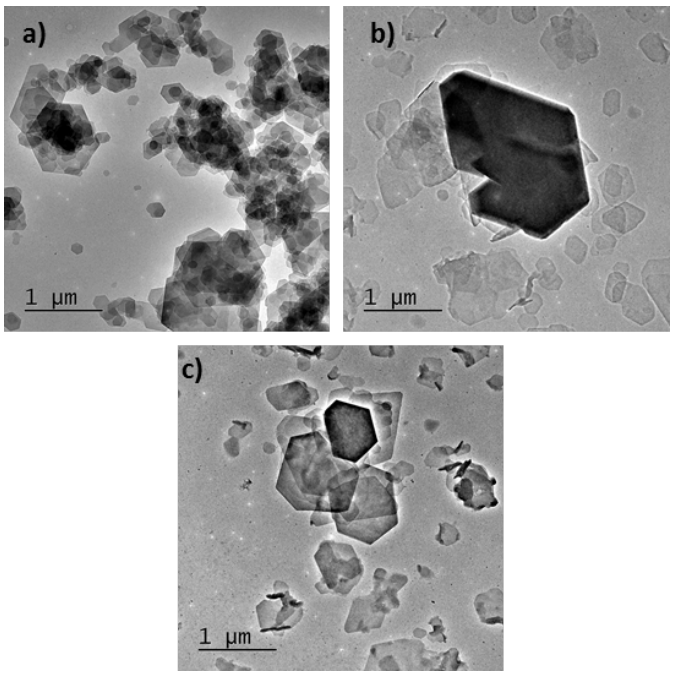

Fig. 6 TEM images of samples left at (a) 8 °C, b)-20 °C and (c) 23 °C for 1 week.

DLS was also used to study the particles size and particles size distribution. When the sample was aged at –20 °C for a week the average particle size increased to 559 nm (Fig. S11). This shows that changing is significantly slowed, or perhaps stopped, when Ca_2AlNO_3-LDH is stored at very low temperatures. The Ca_2AlNO_3-LDH particles left at room temperature (23 °C) appear to be smaller (1449 nm) than the sample left at 8 °C (1865 nm, Fig. S12), which is due to decomposition.

Conclusions

We report an efficient and cost effective method to produce phase pure Ca_2Al-NO_3-LDH nanoplatelets. The as synthesised nanoplatelets have an average particle size of 250 nm (by TEM). The size of the nanoplatelet Ca_2AlNO_3-LDH can be controlled by both the colloidal mill rotor speed and the ageing parameters.

Aqueous suspensions of Ca_2AlNO_3-LDH platelets continue growing post synthesis. TEM data showed that the particles increased in size from 250 to 705 nm in 4 weeks at 8 °C. TEM data also revealed that storage at lower temperatures (-20 °C) significantly slows growth. Ca_2AlNO_3-LDH platelets are not stable in aqueous suspension at room temperature, decomposing to mixed metal oxides and hydroxides.

Experimental details

Synthesis of Ca_2AlNO_3-LDH. 7.56 g of $Ca(NO_3)_2$ and 6.00 g of $Al(NO_3)_3$ (to give a 2:1 Ca:Al ratio of cations) were dissolved in 50 mL of deionised and degassed water (purged with N_2 for two hours to remove any carbonate ions), to give a 0.64 M solution of calcium ions and a 0.32 M solution of aluminium ions. 4.40 g of NaOH pellets were dissolved in another 50 mL of deionised and degassed water to give a 2.2 M solution of NaOH. The colloid mill was first washed with water, and then dionised water three times. The two solutions mentioned above were then poured into the mill for a mixing time of 90 s, the rotor speed was set to 2000 rpm. After mixing the product was collected, washed using deionised and degassed water 4 times using a centrifuge at 9000 rpm for 5 minutes. The sample was then collected, ~0.5 g was dried in a vacuum oven for characterisation, the rest was stored in a fridge at 8 °C.

Acknowledgements

The authors would like to thank SCG Chemicals Co., Ltd, Thailand for financial support, Dr Nicholas H. Rees (University of Oxford) for the solid state NMR experiments, Mr Xian Du (University of Oxford) for XRD analysis.

Notes and references

†Electronic Supplementary Information (ESI) available: [Experimental, Figures and Tables including X-ray diffraction patterns of Ca_2Al-NO_3 LDH with aging times and temperatures, IR, SEM, TEM, BET, solid state NMR, DLS experiments]. See DOI: 10.1039/b000000x/

1 (a) F. Cavani, F. Trifiro and A. Vaccari, Catal. Today, 1991, 11, 173–301. (b) V. Rives, Layered double hydroxides: present and future, Nova Science Publishers, 2001; (c) Q. Wang and D. O'Hare, *Chem. Rev.*, 2012, **112**, 4124. (d) D. G. Evans and X. Duan, *Chem. Commun.*, 2006, 485.
2 E. Manasse, *Atti Soc. Toscana Sci. Nat.*, 1915, 24.
3 D. G. Evans and R. C. T. Slade, Layered Double Hydroxides, Struct Bond, 2006, **119**, 1.
4 A. Pavese, M. Catti, G. Ferraris and S. Hull, *Phys. Chem. Miner.*, 1997, **24**, 85.
5 A. I. Khan and D. O'Hare, *J. Mater. Chem.*, 2002, **12**, 3191–3198.
6 (a) G. Fan, F. Li, D. G. Evans and X. Duan, *Chem. Soc. Rev.*, 2014, **43**, 7040. (b) (a) C. Chen, M. Yang, Q. Wang, J.-C. Buffet and D. O'Hare, *J. Mater. Chem. A*., 2014, **2**, 15102.
7 (a) J.-C. Buffet, N. Wanna, T. A. Q. Arnold, E. K. Gibson, P. P. Wells, Q. Wang, J. Tantirungrotechain and D. O'Hare, *Chem. Mater.*, 2015, **27**, 1495. (b) J.-C. Buffet, Z. R. Turner, R. T. Cooper and D. O'Hare, *Polym. Chem.*, 2015, **6**, 2493. (c) J.-C. Buffet, T. A. Q. Arnold, Z. R. Turner, P. Angpanitcharoen and D. O'Hare, *RSC Advances*, 2015, **5**, 87456.
8 (a) U. Chellam, Z. P. Xu and H. C. Zeng, *Chem. Mater.*, 2000, **12**, 650. (b) S. Gusi, F. Pizzoli, F. Trifiro, A. Vaccari and G. Del Piero, *Stud. Surf. Sci. Catal.*, 1987, **31**, 753.
9 F. Li, Q. Tan, D. G. Evans and X. Duan, *Catal. Letters*, 2005, **99**, 151.
10 D. L. Bish, and A. Livingstone, *Miner. Mag.*, 1981, **44**, 339.
11 P. V. Kamath, *J. Electrochem. Soc.*, 1994, **141**, 2956.
12 V. Rives and M. Angeles Ulibarri, *Coord. Chem. Rev.*, 1999, **181**, 61.
13 (a) R. Sasai, N. Shin'ya, T. Shichi, K. Takagi and K. Gekko, *Langmuir*, 1999, **15**, 413–418. (b) S. Li, J. Lu, M. Wei, D. G. Evans and X. Duan, *Adv. Funct. Mater.*, 2010, **20**, 2848.
14 (a) Q. Wang, J. Undrell, Y. Gao, G. Cai, J.-C. Buffet, C. A. Wilkie and D. O'Hare, *Macromolecules*, 2013, **46**, 6145. (b) Y.

Gao, J. Wu, Q. Wang, C.A. Wilkie, and D. O'Hare, *J. Mater Chem A*., 2014, **2**, 10996.
15 P. C. Pavan, G. de A. Gomes and J. B. Valim, *Microporous Mesoporous Mater.*, 1998, **21**, 659.
16 X. Gao, L. Lei, D. O'Hare, J. Xie, P. Gao and T. Chang, *J. Solid State Chem.*, 2013, **203**, 174.
17 J.-H. Choy, J. Park, S.-Y. Kwak and Y.-J. Jeong, *Angew. Chem. Int. Ed.*, 2000, **39**, 4041.
18 I. Cota, E. Ramírez, F. Medina, J. E. Sueiras, G. Layrac and D. Tichit, *Appl. Clay Sci*., 2010, **50**, 498.
19 M. J. Campos-Molina, J. Santamaría-González, J. Mérida-Robles, R. Moreno-Tost, M. C. G. Albuquerque, S. Bruque-Gámez, E. Rodríguez-Castellón, A. Jiménez-López and P. Maireles-Torres, *Energy Fuels*, 2010, **24**, 979.
20 Y. Kuwahara, K. Tsuji, T. Ohmichi, T. Kamegawa, K. Mori and H. Yamashita, *Catal. Sci. Technol.*, 2012, **2**, 1842.
21 S. Sankaranarayanan, C.A. Antonyraj and S. Kannan, *Bioresour. Technol.*, 2012, **109**, 57.
22 E. López-Salinas, M.E. Ll Serrano, M.A.C. Jácome and I.S. Secora, *J. Porous Mater.*, 1996, **2**, 291.
23 L. Vieille, E.M. Moujahid, C. Taviot-Guého, J. Cellier, J.-P. Besse and F. Leroux, *J. Phys. Chem. Solids*, 2004, **65**, 385.
24 (a) S. Xu, B. Zhang, Z. Chen, J. Yu, D. G. Evans and F. Zhang, *Ind. Eng. Chem. Res*., 2011, **50**, 6567. (b) S. Xu, Z. Chen, B. Zhang, J. Yu, F. Zhang and D. G. Evans, *Chem. Eng. J*., 2009, **155**, 881.
25 (a) L. G. Baquerizo, T. Matschei, K. L. Scrivener, M. Saeidpour and L. Wadso, *Cem. Concr. Res*., 2015, **73**, 143. (b) S. Ng, M. Ezzeldin, P. Mueller-Buschbaum and J. Plank, *Cem. Concr. Res.*, 2013, **54**, 191. (c) J. Plank, N. Zou, Z. Zhao and I. Dekany, *Z. Anorg. Allg. Chem.*, 2014, **640**, 1413. (d) L. Raki, J. J. Beaudoin and L. Mitchell, *Cem. Concr. Res*., 2004, **34**, 1717.
26 L. Vieille, I. Rousselot, F. Leroux, J.-P. Besse and C. Taviot-Guého, *Chem. Mater*., 2003, **15**, 4361.
27 M. Sánchez-Cantú, S. Camargo-Martínez, L. M. Pérez-Díaz, M. E. Hernández-Torres, E. Rubio-Rosas and J. S. Valente, *Appl. Clay Sci.*, 2015, **114**, 509.
28 (a) Y. Zhao, F. Li, R. Zhang, D. G. Evans and X. Duan, *Chem. Mater.*, 2002, **14**, 4286. (b) M. Yang, J. Liu, Z. Chang, G. R. Williams, D. O'Hare, X. Zheng, X. Sun and X. Duan, *J. Mater. Chem.*, 2011, **21**, 14741.
29 (a) A. Pavese, M. Catti, G. Ferraris and S. Hull, *Phys. Chem. Miner.*, 1997, **24**, 85. (b) C. Chen, R. Felton J.-C. Buffet and D. O'Hare, *Chem. Commun*., 2015, **51**, 3462.
30 R. E. Dinneier and S. J. L. Billinge, Principles of Powder Diffraction. In *Powder Diffraction: Theory and Practice*; R. E. Dinneier and S. J. L. Billinge; Eds.; Royal Society of Chemistry, 2008; pp. 1-19.